Chemical Engineering Journal 485 (2024) 149993

Contents lists available at ScienceDirect

Chemical Engineering Journal

journal homepage: www.elsevier.com/locate/cej

Poisoning mechanism of HCl over a Ru-based catalyst for toluene oxidation

Peng Lu, Lyumeng Ye *, Xianhui Yan, Jianhang Huang, Zhixiong Tang, Dongyao Chen, Chaoping Cen *

Guangdong Province Engineering Laboratory for Air Pollution Control, Guangdong Provincial Key Laboratory of Water and Air Pollution Control, South China Institute of Environmental Sciences, MEE, Guangzhou 510655, China

ARTICLE INFO

Keywords:
HCl poisoning
Ru-based catalyst
Toluene catalytic oxidation
Byproducts

ABSTRACT

It is challenging for catalytic oxidation of volatile organic compounds (VOCs) due to the existence of HCl in municipal solid waste incineration flue gases. A thorough probe into the deactivation mechanism is imperative but still lacking. Herein, the poisoning effect of gaseous HCl on a Ru-based catalyst for toluene catalytic oxidation was investigated. Toluene conversion and CO_2 selectivity decreased dramatically from 89.3 % and 93.8 % to 15.0 % and 8.0 %, respectively at 250 °C under HCl atmosphere. HCl led to a reduction of low-temperature redox properties, as well as a decrease of BET surface area, surface oxygen content and mobility, resulting in a loss of catalytic activity. HCl combined with active Ru and Mn, thereby restricting the electron transfer between Ru^{4+} and Mn^{2+}. Moreover, HCl could be oxidized by active oxygen species to form Cl• radical, which subsequently reacted with toluene oxidation intermediates, resulting in the generation of chlorinated compounds, such as chlorobenzene, dichlorobenzene, carbon tetrachloride, and benzyl chloride. These harmful chlorinated compounds predominantly deposited on catalyst surface. The protective role of H_2O against HCl poisoning was mainly attributed to the competitive adsorption between H_2O and Cl ions, the washing effect, and the promoting of intermediates oxidation and oxygen activation. It is noteworthy that during toluene oxidation in the presence of HCl + H_2O, a detectable level of 0.048 ng I-TEQ/Nm^3 PCDD/Fs was observed in the off-gas.

1. Introduction

Volatile organic compounds (VOCs) are widely emitted from industries, causing serious damages to the human health because of their toxicity and carcinogenic effect, and the atmospheric environment due to formation of tropospheric ozone (O_3) and secondary organic aerosol (SOA) [1,2]. The Chinese government is eager to achieve a minimum 10 % reduction in VOCs emission during the 14th five-year plan period (2021–2025). Catalytic oxidation stands out as a highly promising method among the diverse array of technologies available for toluene elimination. This distinction arises from its remarkable efficiency and the relatively low operating temperatures required [3–5]. Available catalysts consist primary of noble metals (e.g., Ru, Ag, Pt), transition metals (e.g., Mn, Cu, Co) and zeolite, etc. Substantial advancements have been achieved in enhancing the catalytic activity of catalysts for toluene oxidation. Nevertheless, given the intricate nature of impurities found in industrial flue gases, the catalysts still face the great challenge of deactivation.

Apart from the typical impurities, such as SO_2, H_2O, alkali metals and heavy metals, the flue gases from municipal solid waste incinerators, coal-fired power plants and some industrial furnaces not only contain above impurities that have extensively studied, but also release HCl sometimes as high as hundreds of ppm [6,7]. Meanwhile, during chlorinated VOCs (CVOCs) deep catalytic oxidation process, C-Cl bond could undergo nucleophilic substitution at Brønsted acidic sites of catalysts, leading to the formation of dissociated Cl. These dissociated Cl species would subsequently participate in a chlorination reaction through Lewis-acid electrophilic substitution, producing Cl-containing byproducts or undergo hydrolysis/oxidation reactions, resulting in HCl/Cl_2 generation [8–10]. Current researches on the design of catalysts for CVOCs oxidation are dedicated to inhibiting the formation of polychlorinated byproducts and improving HCl selectivity [11,12]. As it can be seen, Cl species for CVOCs would be converted into a large amount of gaseous HCl during deep catalytic oxidation process. Although the effect of gaseous HCl on the NH_3-SCR reaction has been intensively investigated [13,14], such an effect on the VOCs catalytic oxidation is quite different. For instance, the gaseous HCl could not only interact with the catalyst, which has great potential to deactivate the catalyst [15,16].

* Corresponding authors.
E-mail addresses: yelvmeng@scies.org (L. Ye), cenchaoping@scies.org (C. Cen).

https://doi.org/10.1016/j.cej.2024.149993
Received 20 December 2023; Received in revised form 8 February 2024; Accepted 24 February 2024
Available online 28 February 2024

Most importantly, it could also engage in organic synthesis process and generate Cl-containing intermediate species, leading to secondary pollution. However, limited research has examined the influence of HCl on VOCs catalytic oxidation process and byproducts generation. A comprehensive understanding of these unknowns is very essential for designing outstanding anti-Cl poisoning catalysts for efficient VOCs removal process in practical applications.

Recently, there has been growing interest in Ru-based catalysts, which have been reported to deliver excellent activity and Cl resistance in CVOCs oxidation due to their great redox property and ability to promote the Deacon reaction [17–22]. MnO_x catalysts are promising for VOCs decomposition because of excellent low-medium temperature activity resulted from variable valance states, high redox ability and oxygen storage capacity [4]. The redox cycles of Ru and Mn in RuO_x-MnO_x composites generate the electron transfer between Ru/Mn oxides, oxygen vacancy and active oxygen species, which contribute to a good catalytic activity [23,24]. In addition, HZSM-5 has been widely used as a carrier owing to adjustable surface acidity, large surface area and thermal/hydrothermal stability [25]. Inspired by these, RuMn/HZSM-5 catalyst may be a good candidate for the investigation of HCl poisoning mechanism on VOCs catalytic oxidation at low-medium temperatures. Toluene is a major component found in industries, such as waste incineration, biomass-burning, sludge incineration, etc [26,27]. There is no chlorine atom(s) in the molecular structure of toluene, which is beneficial to gain an insight into the influence of HCl on VOCs oxidation catalyst and byproducts generation. Therefore, a RuMn/HZSM-5 catalyst and gaseous toluene were chosen as models to explore the influence of gaseous HCl on VOCs catalytic oxidation in this study. The variations in the catalytic activity, the physical and chemical properties of the catalyst before and after poisoning were evaluated. In particular, the solid and gaseous byproducts after the influence of HCl, especially polychlorinated dibenzo-p-dioxins and dibenzofurans (PCDD/Fs), were qualitatively and quantitatively analyzed by gas chromatography coupled with mass spectrometry (GC/MS and HRGC/HRMS). With the assistant of *in-situ* diffuse reflectance infrared Fourier transform spectroscopy (DRIFTs), the possible reaction pathway of toluene oxidation in the presence of gaseous HCl was proposed. This work holds the potential to inform the rational design of catalysts that can efficiently remove VOCs under gaseous HCl with minimum secondary pollution and long-term stability.

2. Experimental

2.1. Catalyst preparation

RuMn/HZSM-5 (denoted as RuMn) catalyst was prepared by a wet impregnation method as described in previous work [25,28]. Certain amounts of $Mn(NO_3)_2$, $RuCl_3{\cdot}xH_2O$ and HZSM-5 were mixed in ethanol and continuously stirred for 5 h, followed by drying at 105 °C for 12 h and calcined at 550 °C in air for 5 h. The precursors $RuCl_3{\cdot}xH_2O$ and $Mn(NO_3)_2$ (AR, 50 wt% in H_2O) were supplied by Shanghai Aladdin Bio-Chem Technology Co., Ltd, China. HZSM-5 with a SiO_2/Al_2O_3 ratio of 25 was purchased from Nankai University Catalyst Co., Ltd, China. The mole ratio of Ru and Mn was 1:1 and the mass ratio of HZSM-5 was 80 wt %. The sample was washed by 12.5 wt% ammonium hydroxide for three times to remove residual Cl from $RuCl_3{\cdot}xH_2O$ during RuMn catalyst preparation. The HCl pretreatment was conducted at 250 °C for 20 h in a gas flow of 50 ppm HCl and balance of N_2. The obtained catalyst after HCl pretreatment was denoted as RuMn-Cl.

2.2. Performance measurement

Toluene (C_7H_8) catalytic oxidation was conducted in a lab-scale fixed-bed quartz tube (i.d. = 8 mm) reactor at 100–350 °C. 200 mL/min feed gas consisted of 50 ppm C_7H_8, 50 ppm HCl, 10 vol% O_2, 5 vol% H_2O and balance of N_2 passed through 0.2 g catalyst, giving a gas hourly space velocity (GHSV) of 60,000 mL/(g•h). The gas composition was monitored by an on-line FTIR spectrometer (GASMET DX-4000). Toluene conversion, CO_2 selectivity and toluene conversion rate were calculated by **Eqs. 1–3**. When calculated the conversion rate in **Eq. (3)**, the toluene conversion was kept below 20 % by applying a high GHSV of 900,000 mL/(g•h) to ensure that all of the catalytic active sites were at operational states [29].

$$Toluene\ conversion(\%) = \left(1 - \frac{C^{out}_{toluene}}{C^{in}_{toluene}}\right) \times 100\% \quad (1)$$

$$CO_2 selectivity(\%) = \frac{C_{CO2}}{7\left(C^{in}_{toluene} - C^{out}_{toluene}\right)} \times 100\% \quad (2)$$

$$\delta_{toluene}\ (\mu mol/(g{\cdot}min)) = \frac{(C^{in}_{toluene} - C^{out}_{toluene}) \times Q}{22.4 \times m} \quad (3)$$

where $C^{in}_{toluene}$(ppm) and $C^{out}_{toluene}$ (ppm) are the toluene concentrations of inlet and outlet of the reactor, C_{CO2} (ppm) is the outlet CO_2 concentration, Q (mL/min) is the gas flow rate, m (mg) is the mass of catalyst.

2.3. Byproducts identification

The outlet gas was collected using a sampling bag (Teflon FEP) and analyzed by GC–MS (Agilent 6890 N GC-5975B MSD). The used catalysts were collected and analyzed using thermal desorption (TD) (APL-TD-2)-GC–MS. TD was operated over ~ 0.1 g sample at 300 °C to desorb the deposited organic byproducts which entered the GC–MS system for identification. The GC oven firstly increased to 150 °C with a heating rate of 5 °C/min and held for 7 min. Afterwards, the GC oven increased to 200 °C with a heating rate of 10 °C/min and held for 4 min. The quadrupole and ion source temperatures were set as 150 °C and 230 °C, respectively.

In the PCDD/F test, the off-gas was collected by absorption in 200 mL toluene for 2 h. The extract was concentrated to approximately 20 μL. The analysis according to EPA method 1613 were conducted using high-resolution gas chromatography/high-resolution mass spectrometer (HRGC/HRMS) on a TRACE 1310 GC coupled to a DFS high resolution magnetic sector MS (Thermo Scientific, USA). The GC temperature program was below: initial oven temperature of 150 °C for 1 min, then increased to 190 °C at 25 °C/min, and finally increased to 280 °C at 3 °C/min and held for 20 min. The MS was operated in an electron impact ionization mode using selected ion monitoring (SIM). The ion source temperature was set at 280 °C. 17 kinds of 2,3,7,8-substituted PCDD/F congeners were detected. The toxic equivalent quantity (TEQ) of the above PCDD/F congeners was calculated using EPA's International Toxicity Equivalent Factor (I-TEF).

2.4. Catalyst characterization

Powder X-ray diffraction (XRD) patterns were recorded using a model D/max RA (Rigaku Co., Japan) in the 2θ range of 10-80° with a step size of 0.02°. N_2 adsorption–desorption experiments were conducted on a chemisorption analyzer (Micromeritics ASAP 2020, USA). Specific surface areas were calculated by the Brunauer-Emmett-Teller (BET) model. Scanning electron microscope (SEM) and energy dispersive spectrometer (EDS) were conducted on ZEISS Gemini SEM 300 coupled with INCA X-Max 80. H_2 temperature programmed reduction (H_2-TPR) and O_2 temperature programmed desorption (O_2-TPD) analyses were carried out using an AutoChem II 2920 instrument. Pyridine adsorbed IR spectroscopy (Py-IR) experiments were carried out by a FTIR spectrometer (PerkinElmer). The calculation methods for the amounts of Brønsted, Lewis and total acid sites were given in **Supporting Information** (**SI**). X-ray photoelectron spectroscopy (XPS) spectra were obtained by Thermo Scientific ESCALAB 250 with Al Kα X-ray radiation (1486.6 eV) operated at 150 W. Electron paramagnetic resonance (EPR) was measured using a Bruker EPR A300 spectrometer,

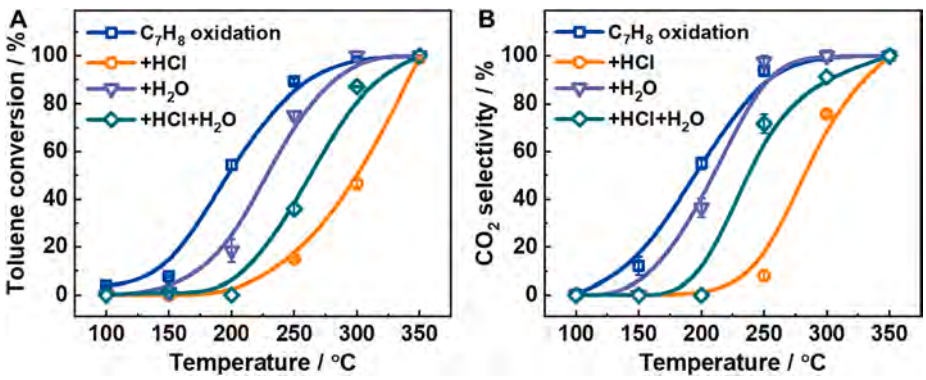

Fig. 1. (A) Toluene conversion and (B) CO_2 selectivity. Reaction condition: [C_7H_8] = 50 ppm, [O_2] = 10 vol%, [H_2O] = 5 vol%, [HCl] = 50 ppm, GHSV = 60,000 mL/(g•h).

which was operated under ultrahigh vacuum at 77 K to increase the quality of the spectra. NH_3 or toluene temperature programmed desorption (TPD) experiments were carried out by the same reactor as activity measurement.

In-situ DRIFTs experiments were conducted using a FTIR spectrometer (Bruker VERTEX 70) equipped with an IR cell with KBr windows and a MCT detector. The sample was pretreated in N_2 at 350 °C for 1 h. Then, the sample was exposed in the experimental atmosphere for 0.5 h to pre-adsorb at a setting temperature and purged the weakly physically adsorbed gases in N_2 for 10 min. Finally, the sample was treated in reaction atmosphere for 0.5 h. Spectra were collected by accumulating 64 scans with a resolution of 4 cm^{-1}. During the DRIFTs experiments, an on-line FTIR spectrometer (GASMET DX-4000) was connected to monitor the composition of outlet gas.

3. Results and discussion

3.1. HCl poisoning on toluene catalytic oxidation performance

Catalytic oxidation of toluene over RuMn at 100–350 °C was carried out. RuMn delivered excellent catalytic performance with low T_{50} and T_{90} (temperatures at which toluene conversions were 50 % and 90 %) of 195.3 °C and 253.7 °C, respectively (Fig. 1**A**). The catalyst experienced significant deactivation in the presence of 50 ppm HCl. Consequently, toluene conversion declined from 89.3 % to 15.0 % at 250 °C, with T_{90} increased to 341.2 °C. Meanwhile, CO_2 selectivity at 250 °C decreased from 93.8 % to 8.0 % (Fig. 1**B**), indicating both the toluene cracking and deep oxidation of intermediates were restrained by HCl.

Since municipal solid waste incineration flue gases also contain H_2O, the influence of H_2O on toluene oxidation performance and HCl poisoning effect were investigated. The effect of H_2O on toluene oxidation was complex, which both contained positive effects of promoting further oxidation of intermediates and oxygen activation, and a negative effect of competitive adsorption on active sites [10,30]. As shown in Fig. 1**A**, the presence of 5 vol% H_2O decreased toluene conversion especially at relatively low temperatures because the competitive adsorption of H_2O and toluene on active sites was more pronounced. When H_2O and HCl were introduced simultaneously, the drop of toluene conversion was less serious than HCl injection alone, which could be explained by following reasons [12,13]. First, previous research reported that H_2O played a role in expediting the removal of Cl species through a washing effect. Second, H_2O may protect the exposure of partial active components to Cl species and inhibit the chlorination of the active metal phase due to competitive adsorption between H_2O and Cl ions, which has been reported in the NH_3-SCR and chlorobenzene oxidation reactions. Third, the OH species generated from H_2O may promote further oxidation of intermediates and oxygen activation. The influence of various water contents on HCl poisoning was further evaluated (Fig. 2**A**). It was observed that the addition of 2–6 vol% H_2O weakened the poisoning effect of HCl on toluene conversion. This positive role was more pronounced at a higher water content. Nevertheless, when water content continuously increased to 8 vol%, the toluene conversion dramatically decreased because excess H_2O molecules may be associated with each other by hydrogen bonds to form water film on catalyst, leading to a recoverable deactivation.

The long-term experiments at 300 °C in Fig. 2**B** showed that HCl decreased toluene conversion dramatically. The presence of H_2O delayed the decreasing tendency of toluene conversion and showed the positive effect on HCl poisoning. After stopping HCl or HCl + H_2O injection at 480 min, the toluene conversion could be gradually recovered. The toluene conversion rate ($\delta_{toluene}$) with different HCl concentrations with/without H_2O were calculated in Fig. 2**C**. In the absence of H_2O,

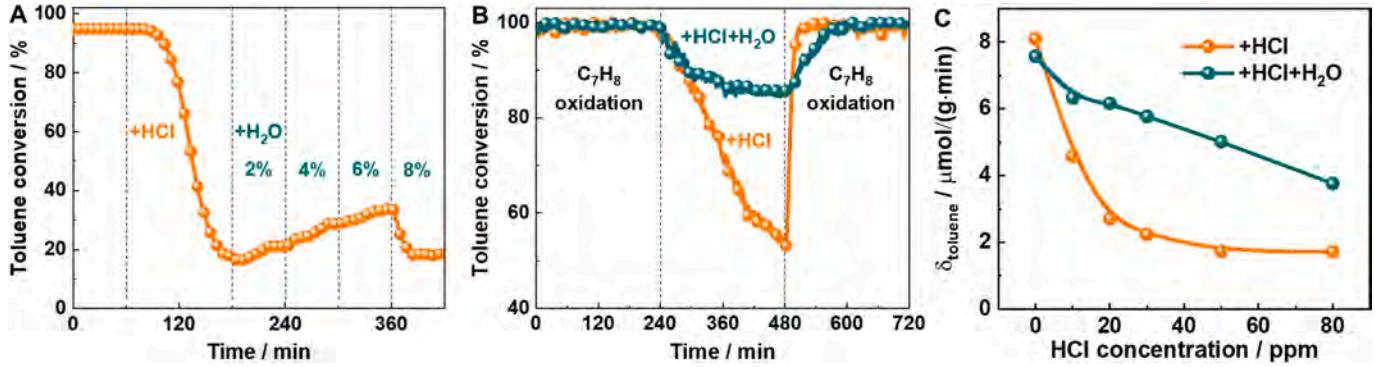

Fig. 2. (A) Different water content gradient experiment (Reaction condition: [C_7H_8] = 50 ppm, [O_2] = 10 vol%, [HCl] = 50 ppm, GHSV = 60,000 mL/(g•h), T = 250 °C). (B) Long-term experiment (Reaction condition: [C_7H_8] = 50 ppm, [O_2] = 10 vol%, [HCl] = 50 ppm, [H_2O] = 5 vol%, GHSV = 60,000 mL/(g•h), T = 300 °C). (C) Toluene conversion rate (Reaction condition: [C_7H_8] = 50 ppm, [O_2] = 10 vol%, [H_2O] = 5 vol%, GHSV = 900,000 mL/(g•h), T = 300 °C).

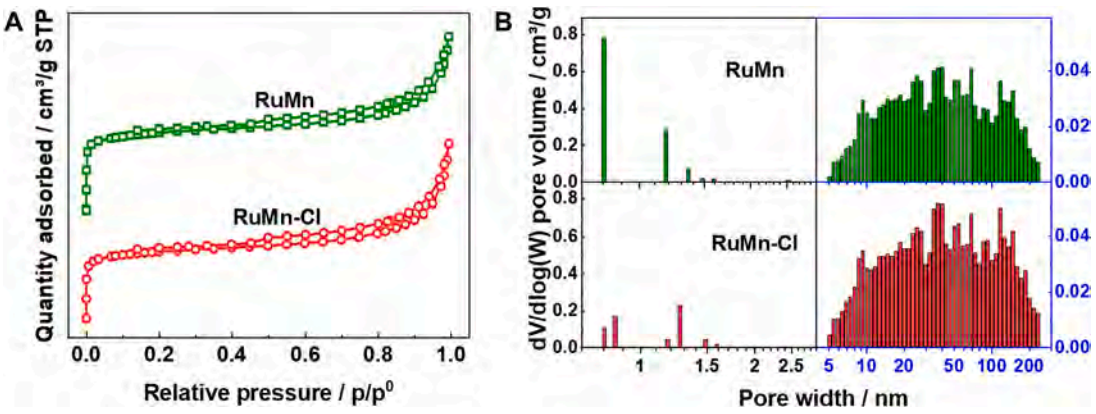

Fig. 3. (A) N_2 adsorption–desorption isotherm and (B) pore size distribution of RuMn and RuMn-Cl.

Table 1
Properties of RuMn and RuMn-Cl.

Catalysts	S^a_{BET} (m^2/g)	V^b_P (cm^3/g)	L^c_{H2} (mmol/g)	T^d_{NH3} (μmol/g)	A^e_B (mmol/g)	A^f_L (mmol/g)	A^g_T (mmol/g)
RuMn	150.7	0.11	6.5	802.8	0.03	0.03	0.06
RuMn-Cl	135.3	0.10	5.1	1238.2	0.03	0.07	0.10

[a,b] Specific surface area and pore volume.
[c] H_2 consumption between 50 and 400 °C from H_2-TPR.
[d] NH_3 desorption amount from NH_3-TPD.
[e,f,g] Amounts of Brønsted, Lewis and total acid sites from Py-IR.

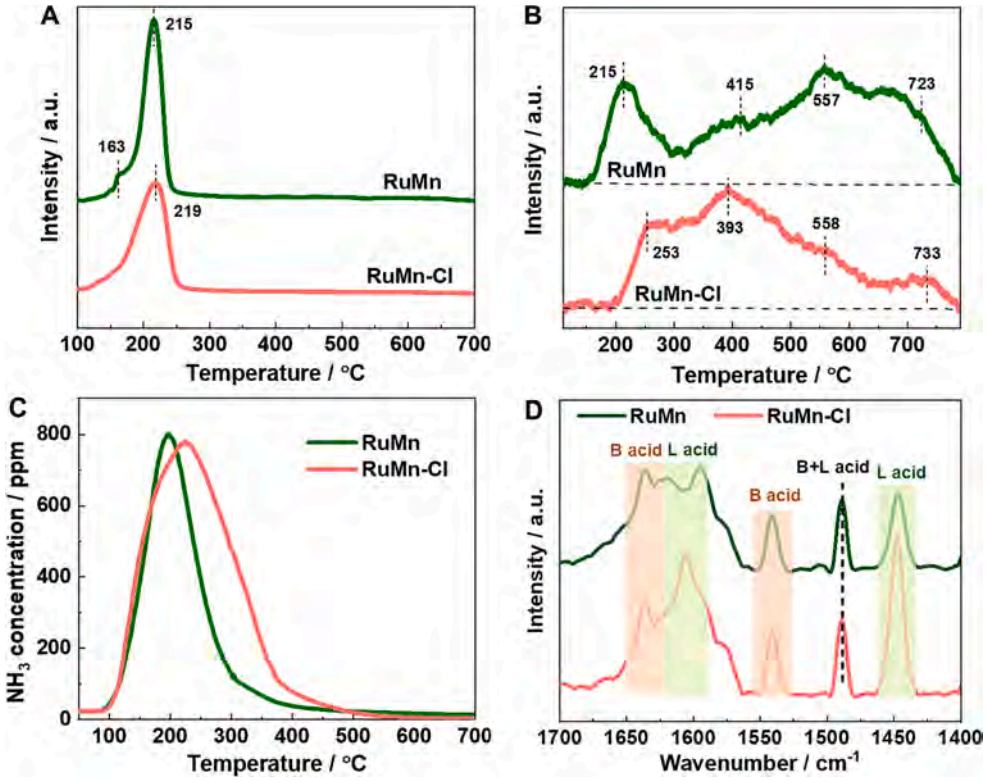

Fig. 4. (A) H_2-TPR, (B) O_2-TPD, (C) NH_3-TPD profiles and (D) Py-IR spectra of RuMn and RuMn-Cl.

when HCl concentration increased from 0 to 80 ppm, $\delta_{toluene}$ decreased dramatically from 8.09 to 1.72 μmol/(g•min). The inhibitory effect of HCl on toluene conversion became worse when increasing HCl concentration. In the presence of 5 vol% H_2O, the $\delta_{toluene}$ decreased from 7.57 to 3.75 μmol/(g•min) with the increasing of HCl concentration from 0 to 80 ppm. The inhibitory effect of HCl was less conspicuous than the situation without H_2O addition, proving again the protective role of H_2O.

3.2. HCl poisoning on physiochemical properties

The RuMn and RuMn-Cl were characterized to investigate the effects

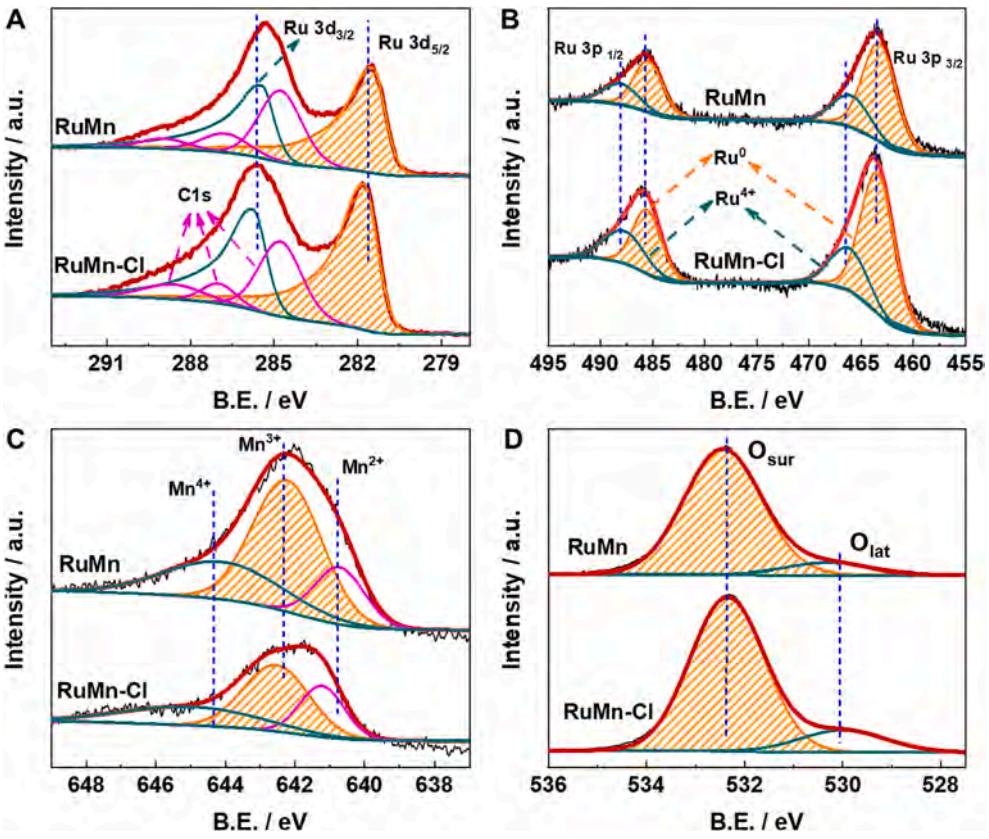

Fig. 5. XPS spectra of (A) Ru 3d, (B) Ru 3p, (C) Mn 2p, (D) O 1s for RuMn and RuMn-Cl.

of HCl on physiochemical properties. As illustrated in **Fig. S1**, the XRD pattern of fresh RuMn exhibited distinctive peaks corresponding to HZSM-5 at angles of 20-30°, 35.9°, 45.4°, and 55.5°, indicating the loading of Ru and Mn did not change the HZSM-5 structure [25]. No obvious reflections attributable to Ru and Mn species were detected, probably due to high dispersion of Ru and Mn species on HZSM-5 support. SEM-EDS mapping images in **Fig. S2** confirmed the uniform dispersion of Ru and Mn on the HZSM-5 support, and the HCl pretreatment increased the Cl content on catalyst surface to 7.8 wt%. After exposure to HCl, the discrepancy in XRD patterns were negligible, suggesting that the possible presence of Cl species as either surface chlorides or amorphous bulk chlorides. The BET surface area and pore volume of RuMn decreased from 150.7 m^2/g and 0.11 cm^3/g to 135.3 m^2/g and 0.10 cm^3/g (Fig. 3 and Table 1), respectively after HCl treatment. The chlorination of the active metals by gaseous HCl may induce the corrosion and a reduction of surface area [12].

The reducibility of catalysts was characterized by H_2-TPR (Fig. 4**A**). A well-defined peak at approximately 215 °C corresponding to the reduction of MnO_2 was observed. The peak at around 163 °C was related to the reduction of Ru^{4+} species including Ru-O-Ru or Ru-O-Mn species [18]. The low-temperature reducibility reflected by the H_2 consumption at 50–400 °C of RuMn-Cl (5.1 mmol/g) was notably weaker than RuMn (6.5 mmol/g). In addition, the reduction peak of MnO_2 over RuMn-Cl slightly shifted to a higher temperature of 219 °C, while the reduction peak of Ru^{4+} species became significantly attenuated. These results indicated that HCl restricted the low-temperature redox ability of RuMn catalyst. Surface oxygen species were subsequently carried out by O_2-TPD (Fig. 4**B**). In the O_2-TPD spectra, the oxygen desorption peaks < 400 °C, 400–700 °C, and > 700 °C can be assigned to chemisorbed peroxy species and monoatomic species (O_{ads}), surface lattice oxygen and bulk lattice oxygen, respectively. Toluene oxidation typically occurs at temperatures ranging from 200 to 400 °C, with O_{ads} species potentially serving as the active oxygen species [30]. The O_{ads} desorption temperature of RuMn-Cl (253 °C) was higher than that of RuMn (215 °C), indicating HCl inhibited the oxygen mobility, which was crucial in catalytic oxidation of toluene.

NH_3-TPD experiments were conducted to analyze the acidity of catalysts (Fig. 4**C**). The desorbed NH_3 amount of RuMn-Cl was 1238.2 μmol/g, much larger than that of RuMn (802.8 μmol/g), indicating an enhancement in catalyst acidity after HCl treatment. This result was further confirmed by Py-IR in Fig. 4**D**. The amounts of Brønsted (B) acids, Lewis (L) acids and total acids in RuMn catalyst were 0.03, 0.03 and 0.06 mmol/g. Chlorine is easily adsorbed on Lewis acid sites, leading to the formation of metallic chlorine and resulting in the accumulation of chlorine on catalyst surface [31]. Thus, the Lewis acids in RuMn would promote the adsorption of HCl and accelerate its toxic effect. Compared with RuMn, the amounts of Lewis acids and total acids in RuMn-Cl increased from 0.03 to 0.07 mmol/g and 0.06 to 0.10 mmol/g, respectively. The partial chlorination of RuO_2 and MnO_x in RuMn catalyst to $RuCl_x$ and $MnCl_x$ could serve as additional Lewis acids and contributed to the formation of Cl-containing organic byproducts as detected by GC–MS (Fig. 9) [15]. Besides, the redox ability of catalyst decreased after HCl treatment as proved by H_2-TPR results. Previous researches already revealed that high acidity without excellent redox properties induces more byproducts formation and deactivation owing to chlorinated byproduct and coke accumulation on the catalyst surface [12]. Therefore, although the amount of acid sites in catalyst was increased in the presence of HCl, the toluene conversion still dropped a lot as verified by performance testing results in Fig. 1.

XPS was adopted to analyze the surface elemental composition and valence states. The overlap between XPS peaks of C 1 s and Ru 3d posed challenges in spectrum assignment for both C and Ru elements (Fig. 5**A**). Thus, Ru 3p in Fig. 5**B** was chosen for the analysis of Ru valence states. The metallic state of Ru (Ru^0) was characterized by the Ru $3p_{3/2}$ peak at 463.5 eV and Ru $3p_{1/2}$ peak at 485.7 eV, whereas Ru^{4+} was characterized by two peaks at 466.4 eV and 488.1 eV [32]. RuMn-Cl exhibited a

Table 2
XPS results of RuMn and RuMn-Cl.

Catalysts	Ru^{4+}/Ru (%)	Mn^{2+}/Mn (%)	Mn^{3+}/Mn (%)	AOS from Mn 3s	O_{sur}/O (%)
RuMn	27.73	17.43	55.79	3.15	91.14
RuMn-Cl	30.13	24.64	47.24	2.41	85.69

higher Ru^{4+} content compared to RuMn. The increased presence of Ru^{4+} species was attributed to the formation of Ru-O-Ru bonds or $RuCl_4$ resulting from chlorination. As for XPS spectra of Mn 2p (Fig. 5**C**), the bands at 641.6, 642.9 and 644.9 eV were assigned to Mn^{2+}, Mn^{3+} and Mn^{4+}, respectively [33]. Upon exposure to HCl, the proportion of Mn^{2+} increased from 17.43 % to 24.64 %, while the Mn^{3+} content decreased from 55.79 % to 47.24 % (Table 2). The charge interaction between Ru^{4+} and Mn^{2+} to generate Ru^0 and Mn^{3+} species play an important role in toluene catalytic oxidation. The increasing contents of Ru^{4+} and Mn^{2+} indicated that the redox cycle of $Ru^{4+} + 4Mn^{2+} \rightleftarrows Ru^0 + 4Mn^{3+}$ was inhibited. This result suggested that the redox property of RuMn catalyst was weakened by HCl, which was in accordance with H_2-TPR results and mainly responsible for the activity decreased. The XPS spectra of Cl 2p were presented in **Fig. S3**. No distinct Cl band was observed for fresh RuMn, suggesting that ammonium hydroxide washing effectively removed the residual Cl species during catalyst preparation. The bands at 198.4 and 200.0 eV in the spectrum of RuMn-Cl were attributed to Cl $2p_{3/2}$ and Cl $2p_{1/2}$ [34]. The O 1s XPS spectra could be fitted into two bands (Fig. 5**D**). The bands at 532.3 and 529.5 eV were related to the surface adsorbed oxygen (O_{sur}, such as O_2^{2-}, O^- and OH^-) and lattice oxygen (O_{lat}), respectively [35]. The O_{sur} is an indicator of the amounts of surface active oxygen. Pretreatment of HCl slightly decreased the O_{sur} content from 91.14 % (RuMn) to 85.69 % (RuMn-Cl).

To investigate the effect of HCl on oxygen vacancy (Vo), the average oxidation state (AOS) of Mn atoms in two samples was calculated. These calculations were based on the multiple splitting of the Mn 3s XPS

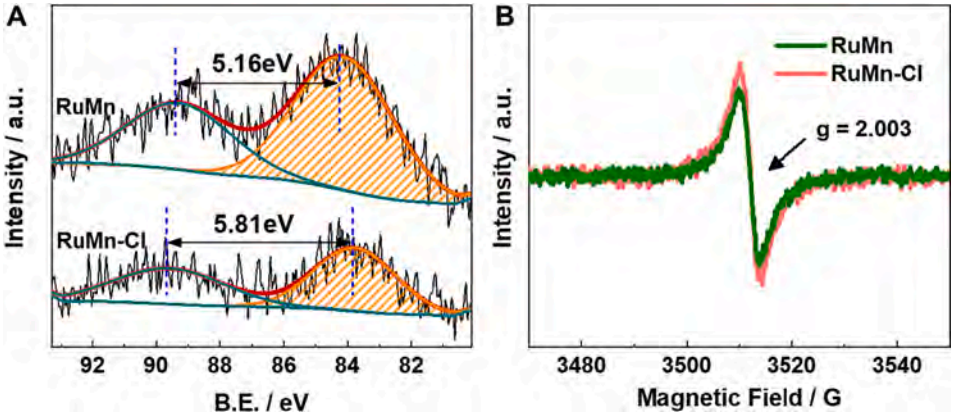

Fig. 6. XPS spectra of (A) Mn 3*s* and (B) low-temperature (77 K) EPR spectra of RuMn and RuMn-Cl.

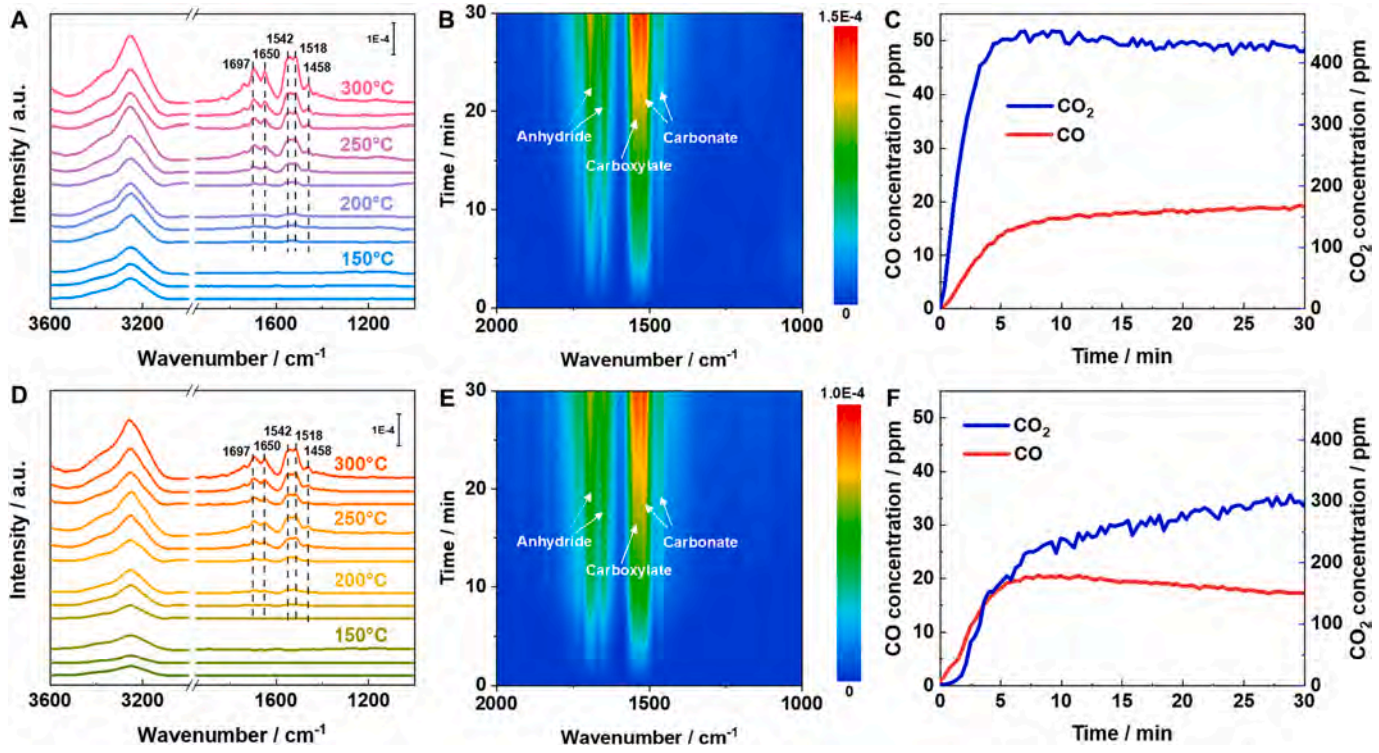

Fig. 7. *In-situ* DRIFTs spectra of toluene oxidation at (A) 150–300 °C and (B) 300 °C, (C) the off-gas composition monitored by FTIR at 300 °C on RuMn, and (D), (E), (F) on RuMn-Cl. Reaction conditions: $[C_7H_8] = 50$ ppm, $[O_2] = 10$ vol%, Q = 100 mL/min for (A), (B), (D) and (E), Q = 300 mL/min and m = 50 mg for (C) and (F).

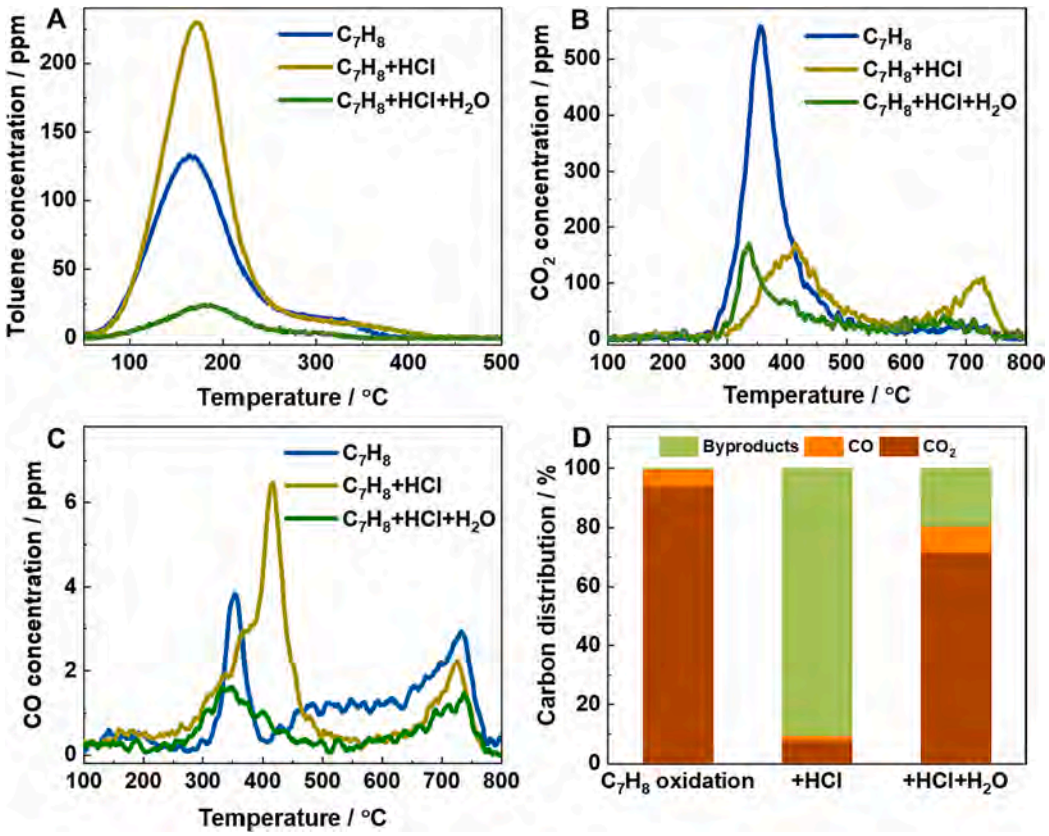

Fig. 8. (A) Toluene-TPD profiles, (B) CO_2 and (C) CO concentrations in toluene-TPD; (D) carbon distribution during toluene oxidation ([C_7H_8] = 50 ppm, [O_2] = 10 vol%, [H_2O] = 5 vol%, [HCl] = 50 ppm, T = 250 °C, GHSV = 60,000 mL/(g•h)).

spectrum (Fig. 6**A**), taking into account the magnitude of the splitting energy (ΔE). The AOS was determined using the formula AOS = 8.956 – 1.126ΔE [35]. The ΔE values of MnRu and MnRu-Cl were 5.16 eV and 5.81 eV, respectively, corresponding to the AOS values of Mn atoms in 3.15 of MnRu and 2.41 of MnRu-Cl. The lower AOS of Mn atoms indicated that a large amount of low-valence Mn atoms exist on the surface. Oxygen vacancy will be generated to maintain electrostatic balance as long as low-valence Mn atoms appeared in the framework of manganese dioxide [35,36]. Low-temperature EPR in vacuum was applied (Fig. 6**B**), and signal at g = 2.003 was originated from the unpaired electron trapped on oxygen vacancy [37,38]. The stronger EPR signal of MnRu-Cl than MnRu indicated much more Vo existed. Both the result of low-temperature EPR and AOS suggested that Cl had been doped into the crystal structure of RuMn, resulting in the formation of oxygen vacancy. The binding energies (BE) of Mn 2p of RuMn showed a slight change after Cl loading, while there was no obvious difference of the Ru 3p. This could be caused by the extension of Mn-O bond as a result of Cl introduction. In addition, the average oxidation state of Mn decreased after the pretreatment with HCl, demonstrating again that Cl ions preferred to incorporate with Mn cations. Consequently, the interaction between Ru and Mn was partially restrained by the toxic effect of HCl on active Mn sites, resulting in a decrease in activity over the RuMn catalyst under gaseous HCl. Besides, HCl restricted the surface oxygen mobility on catalyst (Fig. 4**B**), so the enhancement of oxygen vacancy could not contribute to the catalytic activity.

3.3. In-situ DRIFTs coupled with FTIR

The intermediates of toluene oxidation over RuMn and RuMn-Cl were investigated by *in-situ* DRIFTs coupled with FTIR experiments at first (Fig. 7). The broad band at 3100–3400 cm^{-1} belonged to the O-H stretching vibration in H_2O [2,39]. The bands at 1697 and 1650 cm^{-1} were recognized as the stretching vibration of C = O in aldehyde group [40]. The band at 1542 cm^{-1} belonged to the stretching vibration of $–COO^-$ in carboxylate [41]. The bands at 1518 and 1458 cm^{-1} were ascribed to the stretching vibration of $–COO^-$ in carbonate [42]. Toluene is adsorbed onto the surface initially via the interaction between the methyl group and O_{ads}. After a one-step dehydrogenation to form benzyl alcohol species then probably follow the mechanism [28,43]: benzyl alcohol → benzaldehyde → benzoquinone → maleic anhydride → carbonate → CO_2 and H_2O. The intensity of carbonate (1535 cm^{-1}) was the highest, suggesting the decomposition of carbonates may be the rate-determining step of toluene oxidation at high temperatures [43]. The FTIR results of the off-gas composition at 300 °C were presented in Fig. 7**C and 7F**. As the product of toluene deep oxidation, the highest concentration of CO_2 over RuMn was ~ 450 ppm, which was extremely larger than that of RuMn-Cl (~ 300 ppm). The yield of CO was relatively small (15–20 ppm) but still showed the same tendency as CO_2. These results indicated that HCl could restrain the toluene oxidation process on RuMn catalyst.

3.4. Byproducts analyses

As shown in Fig. 8**A**, the desorbed amount of toluene in TPD experiments was decreased in the order of C_7H_8 + HCl (190.6 μmol/g) > C_7H_8 (132.7 μmol/g) > C_7H_8 + HCl + H_2O (24.3 μmol/g). More toluene could be desorbed in the presence of HCl because HCl reduced the redox capacity of the catalyst, as demonstrated by H_2-TPR. Therefore, the yield of CO_2 + CO from toluene deep oxidation (303.1 μmol/g) was much lower than that from C_7H_8 injection alone (447.2 μmol/g) (Fig. 8**B and 8C**). The CO_2 and CO were mainly generated between 300 and 500 °C by the chemisorbed oxygen species and surface lattice oxygen on catalyst as confirmed by O_2-TPD results in Fig. 4**B**. It was worth noting that the bulk lattice oxygen species appeared over 700 °C, which might play a role in

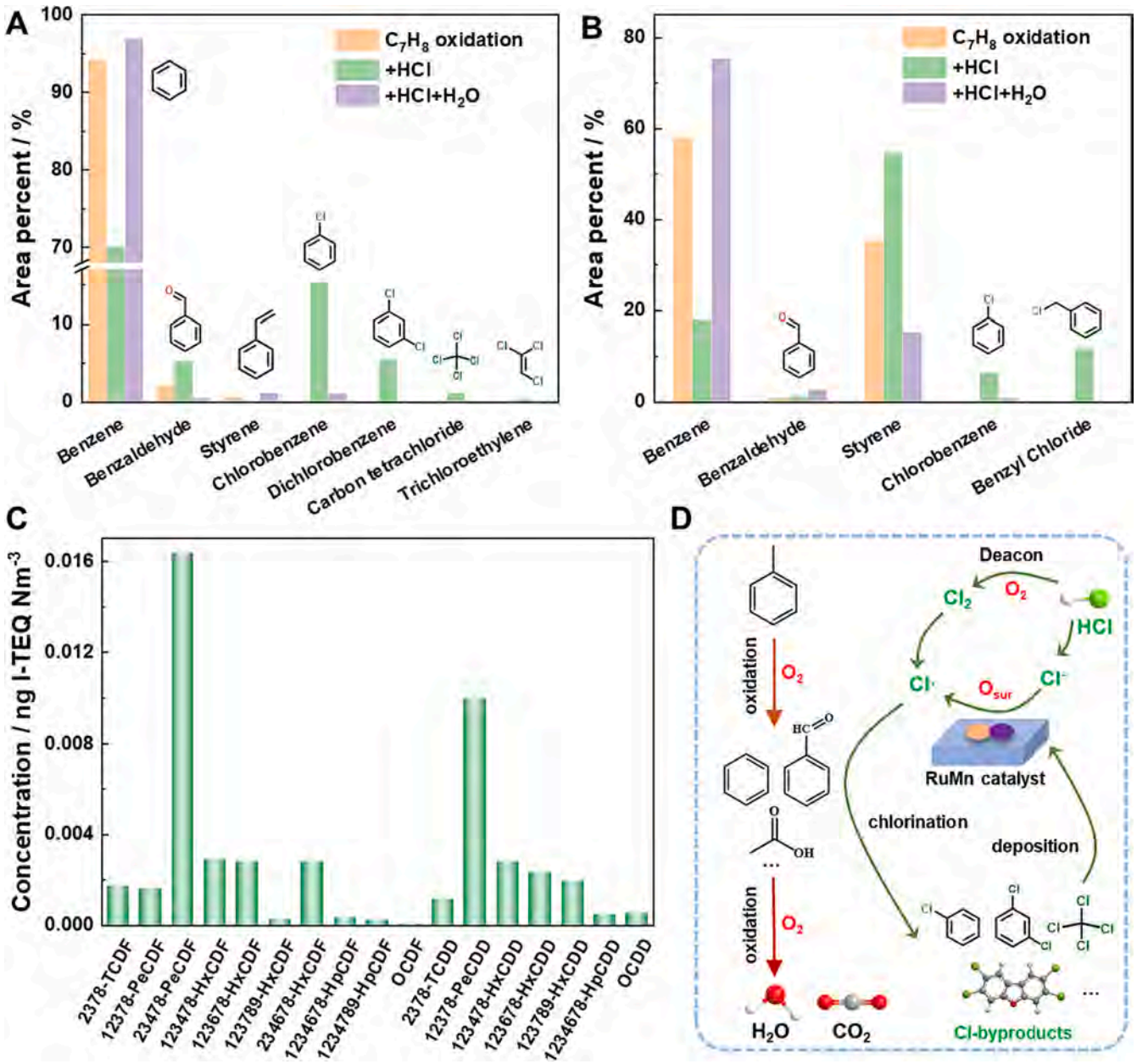

Fig. 9. (A) Distribution of organic species deposited on catalyst surface and (B) distribution of gaseous organic byproducts, (C) I-TEQ concentrations of the 2,3,7,8-substituted PCDD/F congeners in off-gas during toluene catalytic oxidation with HCl and H_2O at 250 °C, (D) possible reaction mechanism of toluene oxidation in the presence of HCl.

further oxidation of the intermediates that were difficult to be decomposed. Therefore, the small CO peaks between 700 and 750 °C may be attributed to the oxidation of intermediates by bulk lattice oxygen species. When HCl and H_2O were introduced simultaneously, both toluene desorption and the CO_2 + CO yield became lowest due to the competitive adsorption between H_2O and toluene on the catalyst surface. The carbon distribution in the off-gas illustrated that HCl reduced the carbon content in CO_2 + CO from 99.7 % to 9.7 % after toluene oxidation at 250 °C, while promoting the distribution of carbon in byproducts to 90.3 % (Fig. 8**D**). However, the co-existence of HCl with H_2O had a positive effect on the complete oxidation of toluene. The proportion of carbon byproducts decreased to only 19.6 % when H_2O and HCl were coexistent, which was significantly lower than that of HCl injection alone.

It was essential to identify the organic species deposited on the catalyst surface. As shown in Fig. 9**A**, benzene (94.15 %) and benzaldehyde (2.20 %) were dominant species of carbon deposition during toluene oxidation at 250 °C. Benzene was typically derived from the demethylation of toluene, while benzaldehyde can be generated by a two-step redox reaction mechanism via partial oxidation of toluene [44]. Upon addition of HCl to the reaction atmosphere, Cl-containing compounds were present, accounting for approximately 23.57 % of the total peak area. Specifically, chlorobenzene (15.42 %), dichlorobenzene (5.47 %), and carbon tetrachloride (1.21 %) were identified. The pathway of chlorination accounted for generating chlorinated compounds via ionic or radical chlorination process. Ionic chlorination involved the electrophilic, consecutive, and selective polarization of Cl_2 into $Cl^{\delta-}$—$Cl^{\delta+}$. Radical chlorination, on the other hand, involved a chain reaction and nonselective dissociation of Cl_2, resulting in two Cl• [22]. For Ru-based catalysts, the Cl• radical chlorination pathway may be dominant. Reactive Cl_2 could be formed by oxidative chlorination between HCl and O_2. The dissociative adsorbed-Cl^- was oxidized to Cl•

radical by active oxygen species on the catalyst surface and chlorinated byproducts were finally formed. The Cl• radical electrophilically substitutes the H• in benzene yielding either chlorobenzene or dichlorobenzene. The electrophilic chlorination reaction may be facilitated by $RuCl_x$ acting as a Lewis acid catalyst, leading to the formation of polychlorinated organic byproducts [45]. Normally, the coke deposition and Cl poisoning are two primary reasons in the deactivation of catalysts [12,46]. Coke mainly originated from toluene in the absence of complete oxidation, which expanded on the external structure and physically blocks pores and active sites. Cl accumulation led to the decline of toluene conversion, resulting from the blockage of pore structures, occupation of active sites and chlorination of metals. The co-existence of HCl and H_2O significantly reduced the content of Cl-containing compounds to approximately 1 %. H_2O hindered the interaction between adsorbed Cl^- species and oxygen species on Vo due to competitive adsorption. H_2O also removed Cl species on catalyst surface by washing effect, resulting in fewer generation of Cl-containing compounds.

The gaseous organic byproducts were analyzed by GC–MS (Fig. 9**B**). Benzene and styrene comprised the primary byproducts (93.35 %) in off-gas during toluene oxidation process. The addition of HCl unavoidably produced chlorinated compounds, including chlorobenzene at 6.53 % and benzyl chloride at 11.73 %, while carbon tetrachloride was scarcely detected. The Cl• radical substituted the H• in the methyl ($–CH_3$) group of toluene, resulting in the production of a significant amount of benzyl chloride. Similar with carbon deposition, the presence of H_2O also reduced the contents of chlorinated compounds in the off-gas. Dioxin formation during toluene oxidation in the presence of HCl and H_2O was another concern. Herein, 17 kinds of 2,3,7,8-substituted PCDD/F congeners after the 24 h test at 250 °C were evaluated. Previous research showed that the PCDD/Fs deposited on the catalyst surface were negligible [44]. Therefore, only those in off-gas would be discussed in this work. As displayed in Fig. 9**C**, the ΣPCDDs, ΣPCDFs and ΣPCDD/Fs were 0.019, 0.029 and 0.048 ng I-TEQ/Nm^3, respectively. The total amount of PCDFs was slightly higher than that of PCDDs. The produced PCDD congener was mostly 1,2,3,7,8-PeCDD, which made up over 50 % of the total PCDDs, while the dominant PCDF congener was 2,3,4,7,8-PeCDF, accounting for more than 55 % of the total PCDFs. Although the gaseous HCl had an unfavorable impact on the formation of PCDD/Fs, the reactive Cl_2 would be formed through the Deacon process ($4HCl + O_2 \leftrightarrow 2Cl_2 + 2H_2O$) [6,47]. Besides, it is well known that the byproducts chlorobenzene or dichlorobenzene identified by GC–MS are important precursors for PCDD/Fs formation [44,48]. The presence of H_2O provided hydrogen for low temperature heterogeneous reactions, and excess hydrogen atoms tended to form low chlorinated dioxin in the chlorination reaction [49]. Hence, there is a potential risk of dioxin generation during toluene catalytic oxidation in the presence of HCl and H_2O, which should receive more attention. Based on the above results, the possible reaction mechanism of toluene oxidation under gaseous HCl atmosphere over RuMn catalyst was finally proposed in Fig. 9**D**.

4. Conclusions

In this study, the HCl poisoning behavior over a Ru-based catalyst for toluene oxidation was investigated. HCl significantly reduced toluene conversion rate and CO_2 selectivity, and the T_{90} of toluene oxidation increased from 253.7 °C to 341.2 °C. The inhibiting effect of HCl was more serious with a higher HCl concentration. The reduction of low-temperature redox ability, BET surface area, surface oxygen content and mobility contributed to the degradation of catalytic activity. Gaseous HCl adsorbed on active Ru and Mn sites to form metal chlorides and thus restricted electron transfer between these metals. Meanwhile, Cl ions were oxidized by active oxygen species to Cl• radical, which reacted with toluene decomposition intermediates to form chlorinated compounds. These harmful organic byproducts mainly deposited on catalyst surface and resulted in deactivation. The PCDD/Fs collected from off-gas were measured as 0.048 ng I-TEQ/Nm^3. Overall, HCl could obviously restrain low-temperature toluene oxidation activity and promote chlorinated byproducts formation. Meanwhile, H_2O could competitively adsorb with Cl ions on active sites and remove deposited chlorinated organic species from the catalyst surface through a washing effect. The OH group generated from H_2O could promote the further oxidation of intermediates and the activation of oxygen. These influences contributed to a protective role of H_2O on HCl poisoning. This study offers insights into the poisoning mechanism of HCl on catalyst properties, intermediates, and chlorinated byproducts over Ru-based catalysts in toluene oxidation, and is expected to contribute to the rational design of anti-Cl poisoning catalysts in practical application.

CRediT authorship contribution statement

Peng Lu: Writing – original draft, Methodology, Investigation, Conceptualization. **Lyumeng Ye:** Writing – review & editing, Methodology. **Xianhui Yan:** Methodology, Investigation. **Jianhang Huang:** Investigation. **Zhixiong Tang:** Resources. **Dongyao Chen:** Investigation. **Chaoping Cen:** Supervision, Methodology, Funding acquisition.

Declaration of competing interest

The authors declare that they have no known competing financial interests or personal relationships that could have appeared to influence the work reported in this paper.

Data availability

The authors do not have permission to share data.

Acknowledgements

This work was supported by the National Key Research and Development Plan of China (2023YFC3707105, 2022YFC3701705), Guangdong Basic and Applied Basic Research Foundation (2022A1515110085), Project of Science and Technology Program of Guangzhou (2024A04J4989), and Central Public-interest Scientific Institution Basal Research Fund of China (PM-zx703-202305-202, PM-zx913-202306-176).

Appendix A. Supplementary data

Supplementary data to this article can be found online at https://doi.org/10.1016/j.cej.2024.149993.

References

[1] X. Zhang, Y. Yang, Q. Zhu, M. Ma, Z. Jiang, X. Liao, C. He, Unraveling the effects of potassium incorporation routes and positions on toluene oxidation over α-MnO_2 nanorods: based on experimental and density functional theory (DFT) studies, J. Colloid Interface Sci. 598 (2021) 324–338.
[2] P. Liu, Y. Liao, J. Li, L. Chen, M. Fu, P. Wu, R. Zhu, X. Liang, T. Wu, D. Ye, Insight into the effect of manganese substitution on mesoporous hollow spinel cobalt oxides for catalytic oxidation of toluene, J. Colloid Interface Sci. 594 (2021) 713–726.
[3] Z. Su, W. Yang, C. Wang, S. Xiong, X. Cao, Y. Peng, W. Si, Y. Weng, M. Xue, J. Li, Roles of oxygen vacancies in the bulk and surface of CeO_2 for toluene catalytic combustion, Environ. Sci. Technol. 54 (2020) 12684–12692.
[4] C. He, J. Cheng, X. Zhang, M. Douthwaite, S. Pattisson, Z. Hao, Recent advances in the catalytic oxidation of volatile organic compounds: a review based on pollutant sorts and sources, Chem. Rev. 119 (2019) 4471–4568.
[5] L. Ye, P. Lu, Y. Peng, J. Li, H. Huang, Impact of NO_x and NH_3 addition on toluene oxidation over MnO_x-CeO_2 catalyst, J. Hazard. Mater. 416 (2021) 125939.
[6] P. Lu, Q. Huang, A.C.T. Bourtsalas, N.J. Themelis, Y. Chi, J. Yan, Review on fate of chlorine during thermal processing of solid wastes, J. Environ. Sci. 78 (2019) 13–28.
[7] A. Dal Pozzo, L. Lazazzara, G. Antonioni, V. Cozzani, Techno-economic performance of HCl and SO_2 removal in waste-to-energy plants by furnace direct sorbent injection, J. Hazard. Mater. 394 (2020) 122518.
[8] J. Wang, X. Wang, X. Liu, T. Zhu, Y. Guo, H. Qi, Catalytic oxidation of chlorinated benzenes over V_2O_5/TiO_2 catalysts: the effects of chlorine substituents, Catal. Today 241 (2015) 92–99.

[9] P. Sun, W. Wang, X. Dai, X. Weng, Z. Wu, Mechanism study on catalytic oxidation of chlorobenzene over $Mn_xCe_{1-x}O_2$/H-ZSM5 catalysts under dry and humid conditions, Appl. Catal., B 198 (2016) 389–397.

[10] Q. Dai, S. Bai, X. Wang, G. Lu, Catalytic combustion of chlorobenzene over Ru-doped ceria catalysts: mechanism study, Appl. Catal., B 129 (2013) 580–588.

[11] Z. Song, S. Yu, H. Liu, Y. Wang, C. Gao, Z. Wang, Y. Qin, Y. Peng, J. Li, Carbon/chlorinate deposition on MnO_x-CeO_2 catalyst in chlorobenzene combustion: the effect of SCR flue gas, Chem. Eng. J. 433 (2022) 133552.

[12] F. Lin, L. Xiang, Z. Zhang, N. Li, B. Yan, C. He, Z. Hao, G. Chen, Comprehensive review on catalytic degradation of Cl-VOCs under the practical application conditions, Crit. Rev. Environ. Sci. Technol. 52 (2020) 311–355.

[13] S. Xiong, J. Chen, N. Huang, T. Yan, Y. Peng, J. Li, The poisoning mechanism of gaseous HCl on low-temperature SCR catalysts: MnO_x-CeO_2 as an example, Appl. Catal., B 267 (2020) 118668.

[14] P. Wang, Q.-S. Wang, X.-X. Ma, R.-T. Guo, W.-G. Pan, The influence of F and Cl on Mn/TiO_2 catalyst for selective catalytic reduction of NO with NH_3: a comparative study, Catal. Commun. 71 (2015) 84–87.

[15] Q. Dai, S. Bai, Z. Wang, X. Wang, G. Lu, Catalytic combustion of chlorobenzene over Ru-doped ceria catalysts, Appl. Catal., B 126 (2012) 64–75.

[16] B. Miranda, E. Díaz, S. Ordóñez, A. Vega, F.V. Díez, Performance of alumina-supported noble metal catalysts for the combustion of trichloroethene at dry and wet conditions, Appl. Catal., B 64 (2006) 262–271.

[17] W. Li, D. Hu, K. Yin, C. Yu, B. Huang, Hierarchical Ru-Ce/H-ZSM-5 catalysts for the catalytic oxidation of chlorobenzene: structure-activity relationship and chlorine poisoning resistance, Surf. Interfaces 34 (2022) 102320.

[18] J. Zhao, W. Xi, C. Tu, Q. Dai, X. Wang, Catalytic oxidation of chlorinated VOCs over Ru/Ti_xSn_{1-x} catalysts, Appl. Catal., B 263 (2020) 118237.

[19] Y. Wang, P. Wang, X. Lu, N. Hu, Q. Wang, S. Wu, W. Deng, L. Wang, Construction of mesoporous Ru@ZSM-5 catalyst for dichloromethane degradation: synergy between acidic sites and redox centres, Fuel 346 (2023) 128337.

[20] X. Lv, M. Jiang, J. Chen, D. Yan, H. Jia, Unveiling the lead resistance mechanism and interface regulation strategy of Ru-based catalyst during chlorinated VOCs oxidation, Appl. Catal., B 315 (2022) 121592.

[21] L. Chen, W. Zhou, C. Huo, L. Li, M. Cui, X. Qiao, Z. Fei, Improved metal-support interaction in Ru/CeO_2 catalyst via plasma-treated strategy for dichloroethane oxidation, Appl. Catal., A 660 (2023) 119215.

[22] Q. Dai, K. Shen, W. Deng, Y. Cai, J. Yan, J. Wu, L. Guo, R. Liu, X. Wang, W. Zhan, HCl-tolerant H_xPO_4/RuO_x-CeO_2 catalysts for extremely efficient catalytic elimination of chlorinated VOCs, Environ. Sci. Technol. 55 (2021) 4007–4016.

[23] Y. Lyu, C. Li, X. Du, Y. Zhu, Y. Zhang, S. Li, Catalytic removal of toluene over manganese oxide-based catalysts: a review, Environ. Sci. Pollut. Res. Int. 27 (2020) 2482–2501.

[24] J. Wang, L. Dai, J. Deng, Y. Liu, L. Jing, X. Hao, W. Pei, X. Yu, A. Rastegarpanah, H. Dai, An investigation on catalytic performance and reaction mechanism of RuMn/meso-TiO_2 derived from RuMn intermetallic compounds for methyl ethyl ketone oxidation, Appl. Catal., B 296 (2021).

[25] P. Lu, L. Ye, X. Yan, P. Fang, X. Chen, D. Chen, C. Cen, Impact of toluene poisoning on MnCe/HZSM-5 SCR catalyst, Chem. Eng. J. 414 (2021) 128838.

[26] P. Lu, L. Ye, X. Yan, X. Chen, P. Fang, D. Chen, D. Chen, C. Cen, Insight into the promotional effect of NO_2 on toluene oxidation over MnCe/HZSM-5 catalyst, Appl. Surf. Sci. 600 (2022) 154161.

[27] L. Ye, P. Lu, X. Chen, P. Fang, Y. Peng, J. Li, H. Huang, The deactivation mechanism of toluene on MnO_x-CeO_2 SCR catalyst, Appl. Catal., B 277 (2020) 119257.

[28] P. Lu, L. Ye, X. Yan, D. Chen, D. Chen, X. Chen, P. Fang, C. Cen, Performance of toluene oxidation over MnCe/HZSM-5 catalyst with the addition of NO and NH_3, Appl. Surf. Sci. 567 (2021) 150836.

[29] G. Li, K. Shen, L. Wang, Y. Zhang, H. Yang, P. Wu, B. Wang, S. Zhang, Synergistic degradation mechanism of chlorobenzene and NO over the multi-active center catalyst: the role of NO_2, brønsted acidic site, oxygen vacancy, Appl. Catal., B 286 (2021) 119865.

[30] X. Zhang, F. Bi, Z. Zhu, Y. Yang, S. Zhao, J. Chen, X. Lv, Y. Wang, J. Xu, N. Liu, The promoting effect of H_2O on rod-like $MnCeO_x$ derived from MOFs for toluene oxidation: a combined experimental and theoretical investigation, Appl. Catal., B 297 (2021) 120393.

[31] H. Wang, B. Peng, R. Zhang, H. Chen, Y. Wei, Synergies of mn oxidative ability and ZSM-5 acidity for 1, 2-dichloroethane catalytic elimination, Appl. Catal., B 276 (2020) 118922.

[32] V.B. Saptal, T. Sasaki, B.M. Bhanage, Ru@PsIL-catalyzed synthesis of N-formamides and benzimidazole by using carbon dioxide and dimethylamine borane, ChemCatChem 10 (2018) 2593–2600.

[33] J.-R. Li, W.-P. Zhang, C. Li, H. Xiao, C. He, Insight into the catalytic performance and reaction routes for toluene total oxidation over facilely prepared Mn-Cu bimetallic oxide catalysts, Appl. Surf. Sci. 550 (2021) 149179.

[34] Q. Wang, F. Lin, J. Zhou, J. Zhang, J. Jin, Effect of HCl and o-DCBz on NH_3-SCR of NO over MnO_x/TiO_2 and MnO_x-CeO_2/TiO_2 catalysts, Appl. Catal., A 605 (2020) 117801.

[35] B. Zhang, J. Ji, B. Liu, D. Zhang, S. Liu, H. Huang, Highly efficient ozone decomposition against harsh environments over long-term stable amorphous MnO_x catalysts, Appl. Catal., B 315 (2022) 121552.

[36] G. Zhu, W. Zhu, Y. Lou, J. Ma, W. Yao, R. Zong, Y. Zhu, Encapsulate alpha-MnO_2 nanofiber within graphene layer to tune surface electronic structure for efficient ozone decomposition, Nat. Commun. 12 (2021) 4152.

[37] Y. Fang, H. Li, Q. Zhang, C. Wang, J. Xu, H. Shen, J. Yang, C. Pan, Y. Zhu, Z. Luo, Y. Guo, Oxygen vacancy-governed opposite catalytic performance for C_3H_6 and C_3H_8 combustion: the effect of the Pt electronic structure and chemisorbed oxygen species, Environ. Sci. Technol. 56 (2022) 3245–3257.

[38] J. Yang, S. Hu, L. Shi, S. Hoang, W. Yang, Y. Fang, Z. Liang, C. Pan, Y. Zhu, L. Li, J. Wu, J. Hu, Y. Guo, Oxygen vacancies and Lewis acid sites synergistically promoted catalytic methane combustion over perovskite oxides, Environ. Sci. Technol. 55 (2021) 9243–9254.

[39] J. Zhong, Y. Zeng, D. Chen, S. Mo, M. Zhang, M. Fu, J. Wu, Z. Su, P. Chen, D. Ye, Toluene oxidation over Co^{3+}-rich spinel Co_3O_4: evaluation of chemical and by-product species identified by in situ DRIFTS combined with PTR-TOF-MS, J. Hazard. Mater. 386 (2020) 121957.

[40] Z. Hou, X. Zhou, T. Lin, Y. Chen, X. Lai, J. Feng, M. Sun, The promotion effect of tungsten on monolith Pt/$Ce_{0.65}Zr_{0.35}O_2$ catalysts for the catalytic oxidation of toluene, New J. Chem. 43 (2019) 5719–5726.

[41] L. Zhao, Z. Zhang, Y. Li, X. Leng, T. Zhang, F. Yuan, X. Niu, Y. Zhu, Synthesis of Ce_aMnO_x hollow microsphere with hierarchical structure and its excellent catalytic performance for toluene combustion, Appl. Catal., B 245 (2019) 502–512.

[42] X. Chen, X. Chen, S. Cai, E. Yu, J. Chen, H. Jia, MnO_x/Cr_2O_3 composites prepared by pyrolysis of Cr-MOF precursors containing in situ assembly of MnO_x as high stable catalyst for toluene oxidation, Appl. Surf. Sci. 475 (2019) 312–324.

[43] W. Yang, Z.a. Su, Z. Xu, W. Yang, Y. Peng, J. Li, Comparative study of α-, β-, γ- and δ-MnO_2 on toluene oxidation: oxygen vacancies and reaction intermediates, Appl. Catal., B 260 (2020) 118150.

[44] W. Jiang, Y. Yu, F. Bi, P. Sun, X. Weng, Z. Wu, Synergistic elimination of NO_x and chloroaromatics on a commercial V_2O_5-WO_3/TiO_2 catalyst: byproduct analyses and the SO_2 effect, Environ. Sci. Technol. 53 (2019) 12657–12667.

[45] S. Zhai, Y. Su, X. Weng, R. Li, H. Wang, Z. Wu, Synergistic elimination of NO_x and chlorinated organics over VO_x/TiO_2 catalysts: a combined experimental and DFT study for exploring vanadate domain effect, Environ. Sci. Technol. 55 (2021) 12862–12870.

[46] A. Aranzabal, J.A. González-Marcos, M. Romero-Sáez, J.R. González-Velasco, M. Guillemot, P. Magnoux, Stability of protonic zeolites in the catalytic oxidation of chlorinated VOCs (1,2-dichloroethane), Appl. Catal., B 88 (2009) 533–541.

[47] F. Zhou, Q. Xin, Y. Fu, Z. Hua, Y. Dong, M. Ran, H. Song, S. Liu, R. Qu, Y. Yang, X. Zhang, C. Zheng, X. Gao, Efficient catalytic oxidation of chlorinated volatile organic compounds over RuO_2-WO_x/$Sn_{0.2}Ti_{0.8}O_2$ catalysts: insight into the Cl poisoning mechanism of acid sites, Chem. Eng. J. 464 (2023) 142471.

[48] D. Wang, Q. Chen, X. Zhang, C. Gao, B. Wang, X. Huang, Y. Peng, J. Li, C. Lu, J. Crittenden, Multipollutant control (MPC) of flue gas from stationary sources using SCR technology: a critical review, Environ. Sci. Technol. 55 (2021) 2743–2766.

[49] K. Shao, J. Yan, X. Li, S. Lu, Y. Wei, M. Fu, Experimental study on the effects of H_2O on PCDD/Fs formation by de novo synthesis in carbon/$CuCl_2$ model system, Chemosphere 78 (2010) 672–679.